



Multiple solitary wave interactions

Nakayama, Keisuke

Tsuji, Hidekazu

(Citation)

Physics of Fluids, 33(8):086602

(Issue Date)

2021-08

(Resource Type)

journal article

(Version)

Version of Record

(Rights)

© 2021 Author(s). Published under an exclusive license by AIP Publishing. This article may be downloaded for personal use only. Any other use requires prior permission of the author and AIP Publishing. This article appeared in Physics of Fluids 33, 086602, (2021) and may be found at <https://doi.org/10.1063/5.0056258>

(URL)



<https://hdl.handle.net/20.500.14094/90008599>



Multiple solitary wave interactions

Cite as: Phys. Fluids **33**, 086602 (2021); <https://doi.org/10.1063/5.0056258>

Submitted: 07 May 2021 . Accepted: 15 July 2021 . Published Online: 05 August 2021

 Keisuke Nakayama (中山恵介), and  Hidekazu Tsuji (辻英一)



View Online



Export Citation



CrossMark

ARTICLES YOU MAY BE INTERESTED IN

[Tsunami resonance and standing waves in Hangzhou Bay](#)

Physics of Fluids **33**, 081702 (2021); <https://doi.org/10.1063/5.0059383>

[Will we ever wash our hands of lubrication theory?](#)

Physics of Fluids **33**, 081908 (2021); <https://doi.org/10.1063/5.0060307>

[Stability of buoyancy-driven flow in a vertical channel with one heated wall](#)

Physics of Fluids **33**, 084103 (2021); <https://doi.org/10.1063/5.0059757>

Physics of Fluids

SPECIAL TOPIC: Flow and Acoustics of Unmanned Vehicles

Submit Today!

Multiple solitary wave interactions

Cite as: Phys. Fluids **33**, 086602 (2021); doi: [10.1063/5.0056258](https://doi.org/10.1063/5.0056258)

Submitted: 7 May 2021 · Accepted: 15 July 2021 ·

Published Online: 5 August 2021



View Online



Export Citation



CrossMark

Keisuke Nakayama (中山恵介),^{1,a)} and Hidekazu Tsuji (辻英一)²

AFFILIATIONS

¹Kobe University, 1-1 Rokkodai-Cho, Nada-Ku, Kobe, Hyogo, 657-8501, Japan

²Kyushu University, 6-1 Kasuga-Koen, Kasuga, Fukuoka, 816-8580, Japan

^{a)}Author to whom correspondence should be addressed: nakayama@phoenix.kobe-u.ac.jp

ABSTRACT

Theoretical solutions of two-soliton resonance show the possibility that the amplitude of soliton resonance is four times as large as the incident solitary wave at the critical angle. The two-soliton interaction with a symmetrical configuration is generally categorized into (3142)-type and (2143)-type (O-type). Previous studies demonstrated that amplification factors of (3142)-type and O-type are successfully reproduced by using a function of the modified Miles' prediction, κ , in which (3142)-type and O-type correspond to $0 < \kappa < 1$ and $\kappa > 1$. However, a train of solitary waves often occurs in shallow water, resulting in multiple solitary wave interactions. Therefore, it is necessary to investigate the interaction of multiple solitary waves due to soliton resonance. We, thus, applied theoretical solutions to analyze the interaction of multiple solitary waves, which was validated by using numerical simulations based on the variational principle. It was revealed that the second and the subsequent soliton resonances are O-type when κ is larger than zero.

Published under an exclusive license by AIP Publishing. <https://doi.org/10.1063/5.0056258>

I. INTRODUCTION

Miles (1977) demonstrated theoretical solutions of two soliton resonance by considering the reflection of a solitary wave from the oblique wall with an incident angle, which is the so-called Miles' prediction. The theory showed that the amplitude of soliton resonance is four times as large as the incident solitary wave at the critical angle (Melville, 1980). Mach reflection occurs due to soliton resonance when an incident angle is less than the critical angle in which the third solitary wave (stem) appears. From a practical viewpoint, Peterson *et al.* (2003) suggested that "Freak waves" are associated with the soliton resonance that occurs due to the interaction of two solitary waves (Kharif and Pelinovsky, 2003; Soomere and Engelbrecht, 2005). Funakoshi (1980) applied the Boussinesq equations to compute an incident solitary wave propagating along the oblique boundary with an incident angle, which supported the Miles' prediction under the weakly nonlinear condition. Tanaka (1993) investigated the oblique reflection of a large-amplitude solitary wave numerically, which showed that the amplification factor is about three (Yeh *et al.*, 2010; Li *et al.*, 2011; Gidel *et al.*, 2017). Kodama (2010, 2016) proposed a modified Miles' prediction based on the Kadomtsev–Petviashvili (KP) equation, which showed that the previous laboratory and numerical results agreed well with the modified Miles' prediction (Tanaka, 1993; Nakayama *et al.*, 2019).

Previous studies have shown that soliton resonance occurs due to the interaction of internal solitary waves similar to surface waves

(Shimizu and Nakayama, 2017). Shimizu and Nakayama (2017) showed the occurrence of large-amplitude internal solitary waves due to soliton resonance in the Andaman Sea by using a non-hydrostatic numerical model. Additionally, Helfrich and Melville (2006) demonstrated the interaction of internal solitary waves by using synthetic aperture radar images. Regarding large-amplitude internal solitary waves, many images reveal the presence of solitary waves that have substantial amplitudes (Wang and Pawlowicz, 2012; Xue *et al.*, 2013). On a laboratory scale, Maxworthy (1980) demonstrated the occurrence of the Mach stem due to the interaction of two internal solitary waves. Tsuji and Oikawa (2007) and Nakayama *et al.* (2019) showed the suppression of amplification due to soliton resonance in a two-layer system by applying critical depth based on the KP equation.

In regard to the large-amplitude solitary waves that may cause soliton resonance, Horn *et al.* (2000, 2002) showed that large-amplitude internal solitary waves may occur as a train of solitary waves. They carried out laboratory experiments using a tilting tank, which demonstrated that low-frequency internal waves are transformed into high-frequency internal solitary waves (a train of internal solitary waves). The occurrence of the train of internal solitary waves was confirmed by applying a fully nonlinear and strongly dispersive internal wave model in a two-layer system (FDI-2s) (Nakayama and Kakinuma, 2010; Nakayama *et al.*, 2019). Shimizu and Nakayama (2017) also demonstrated that a train of internal solitary waves may cause soliton resonance in the Andaman Sea (Zheng *et al.*, 1995). For

surface waves, a train of solitary waves was found to occur and induce soliton resonance due to the reflection from the riverbank when a tsunami penetrates into a meandering river (Nakayama *et al.* 2016). Therefore, it is crucial to investigate the interaction of multiple solitary waves and clarify the mechanisms of soliton resonance.

A train of solitary waves often generates multiple solitary wave interactions in shallow water, but few studies attempted to investigate the interactions. Also, strong nonlinearity may affect the interaction of multiple solitary waves due to soliton resonance. Therefore, we need to consider nonlinearity accurately, such as by a three-dimensional non-hydrostatic model (Nakayama, 2006; Aghsaei *et al.*, 2010; Arthur and Fringer, 2014; Shimizu and Nakayama, 2017; Nakayama *et al.*, 2019). However, the full three-dimensional non-hydrostatic model includes viscosity and turbulence. To analyze the interaction of solitary waves in direct comparison with theoretical solutions, the FDI-2s is considered to be one of the most suitable models because the FDI-2s is a layer model from which it is possible to remove energy dissipation due to viscosity. Although the FDI-2s was designed to analyze the internal waves in a two-layer system, it can also be used to analyze surface water waves by considering that the upper and lower layers are air and water layers, respectively. Thus, we applied the FDI-2s to investigate the interaction of multiple solitary waves due to soliton resonance. First, we investigated the applicability of the modified Miles' prediction to the first soliton resonance generated from the oblique boundary. Second, we hypothesized that the second and the subsequent soliton resonances can be classified into (2143)-type (O-type), which we verified theoretically and numerically. Finally, we proposed theoretical solutions to estimate the amplification factors due to the interaction of multiple solitary waves.

II. ANALYSIS OF WEAKLY NONLINEAR THEORY

A. Reflection of the first solitary surface wave due to an oblique boundary (first soliton resonance)

The Wronskian formulation yields multi-soliton solutions for the KP equation, $\partial/\partial x(4\partial\hat{u}/\partial\hat{t} + 6\hat{u}\partial\hat{u}/\partial\hat{x} + \partial^3\hat{u}/\partial\hat{x}^3) + 3\partial^2\hat{u}/\partial\hat{y}^2 = 0$ with $\hat{u} = 3u/(2h)$, $\hat{x} = (x - c_0)t/h$, $\hat{y} = y/h$, and $\hat{t} = 2c_0t/(3h)$ in the water surface displacement of u , the total water depth of h , the longwave speed of c_0 , the time of t , the propagation direction of x , the orthogonal direction to x of y (Kodama, 2010). For example, soliton interaction generated from the oblique boundary may be classified into three types—(3142)-type, (2143)-type (O-type), and (4321)-type (P-type) (Fig. 1). $[i, j]$ indicates the $[i, j]$ -soliton with the amplitude of $(k_j - k_i)^2/2$ and the $[i, j]$ -soliton angle of $\tan(k_i + k_j)$, in which k_i and k_j are the soliton parameters. (3142)-type shows the typical example of soliton resonance: generation of soliton $[1, 4]$, by interacting two solitons, $[1, 3]$ and $[2, 4]$. It provides evidence that soliton reflection at the boundary can be explained by soliton resonance with a symmetric configuration for the main propagation direction.

We attempted to investigate multiple solitary waves with amplitudes of $a_1, a_2, a_3, \dots, a_i$, which are reflected from the oblique boundary with an incident angle of θ_1 (Fig. 2). The non-dimensional amplitude and angle are given as $\alpha_i = 3a_i/(2h)$ and $\gamma_i = \tan(\theta_i)$. According to Kodama (2010), (3142)-type satisfies the following relationships, $\gamma_{1KP} < \sqrt{2\alpha_{1KP}}$, and $k_{1(3142)} < k_{2(3142)} < k_{3(3142)} < k_{4(3142)}$ as follows:

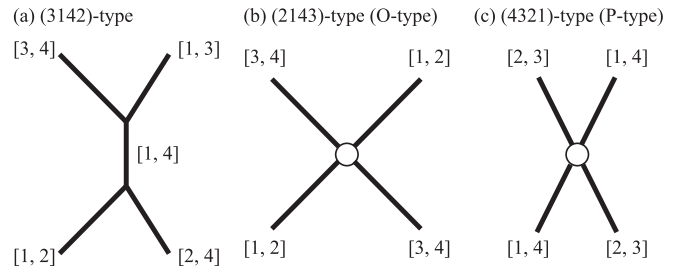


FIG. 1. The schematic diagram for three types of two-soliton interaction. (a) (3142)-type. (b) (2143)-type (O-type). (c) (4321)-type (P-type). $[i, j]$ indicates the $[i, j]$ -soliton. (3142)-type is soliton resonance, and circles are local interaction with a phase shift of solitons. Note that the selection of the type depends on not only the angles but also the soliton parameters.

$$k_{1(3142)} = -\frac{\gamma_1}{2} - \sqrt{\frac{\alpha_{1KP}}{2}}, \quad (1)$$

$$k_{2(3142)} = \frac{\gamma_1}{2} - \sqrt{\frac{\alpha_{1KP}}{2}}, \quad (2)$$

$$k_{3(3142)} = -\frac{\gamma_1}{2} + \sqrt{\frac{\alpha_{1KP}}{2}}, \quad (3)$$

$$k_{4(3142)} = \frac{\gamma_1}{2} + \sqrt{\frac{\alpha_{1KP}}{2}}, \quad (4)$$

$$\alpha_{R1KP} = \frac{\gamma_1^2}{2}, \quad (5)$$

$$\gamma_{R1} = \sqrt{2\alpha_{1KP}}, \quad (6)$$

$$\alpha_{A1KP} = \alpha_{1KP} \left(1 + \frac{\gamma_1}{\sqrt{2\alpha_{1KP}}} \right)^2, \quad (7)$$

$$\gamma_W = \gamma_1 \frac{1 - \gamma_1/\sqrt{2\alpha_{1KP}}}{3\gamma_1/\sqrt{2\alpha_{1KP}}}, \quad (8)$$

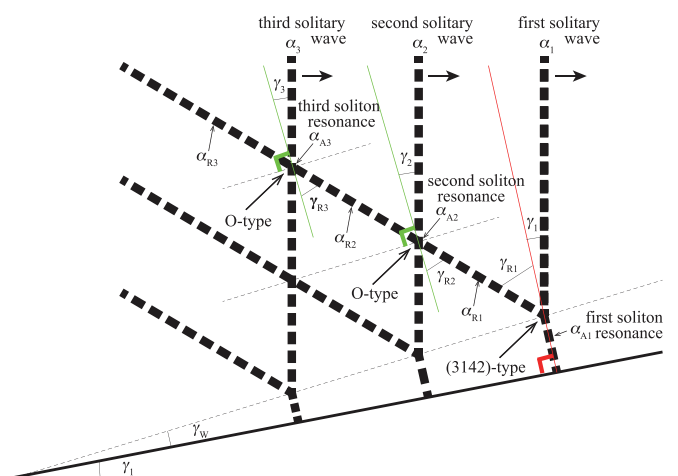


FIG. 2. Schematic diagram of the oblique reflection of multiple solitary waves. In the case depicted, the first solitary wave reflects from the oblique boundary as (3142)-type and the next solitary waves are of O-type with the reflection of the first soliton wave.

where α_{1KP} is the non-dimensional incident amplitude for the KP theory, α_{R1KP} is the non-dimensional amplitude of the reflection of the first solitary wave from the oblique boundary for the KP theory, γ_{R1} is the non-dimensional angle of the reflection of the first solitary wave from the oblique boundary, γ_w is the non-dimensional angle due to extension of the Mach stem, α_{A1KP} is the non-dimensional amplitude of the first soliton resonance for the KP theory, and $k_{1(3142)}$, $k_{2(3142)}$, $k_{3(3142)}$, and $k_{4(3142)}$ are the parameters for the first soliton resonance.

On the other hand, O-type satisfies $\gamma_{1KP} > \sqrt{2\alpha_{1KP}}$ and $k_{1(2143)} < k_{2(2143)} < k_{3(2143)} < k_{4(2143)}$ as follows:

$$k_{1(2143)} = -\frac{\gamma_1}{2} - \sqrt{\frac{\alpha_{1KP}}{2}}, \quad (9)$$

$$k_{2(2143)} = -\frac{\gamma_1}{2} + \sqrt{\frac{\alpha_{1KP}}{2}}, \quad (10)$$

$$k_{3(2143)} = \frac{\gamma_1}{2} - \sqrt{\frac{\alpha_{1KP}}{2}}, \quad (11)$$

$$k_{4(2143)} = \frac{\gamma_1}{2} + \sqrt{\frac{\alpha_{1KP}}{2}}, \quad (12)$$

$$\alpha_{R1KP} = \alpha_{1KP}, \quad (13)$$

$$\gamma_{R1} = \gamma_1, \quad (14)$$

$$\alpha_{A1KP} = \frac{4\alpha_{1KP}}{1 + \sqrt{1 - (\sqrt{2\alpha_{1KP}}/\gamma_1)^2}}, \quad (15)$$

$$\gamma_w = 0, \quad (16)$$

where $k_{1(2143)}$, $k_{2(2143)}$, $k_{3(2143)}$, and $k_{4(2143)}$ are the parameters for the first soliton resonance.

Kodama (2010) proposed to improve Miles' prediction (the modified Miles' prediction) for the case that two solitary waves with the same amplitude interact as follows:

$$\alpha_{1KP} = \alpha_1 \cos^2 \theta_1 = \alpha_1 \frac{1}{1 + \gamma_1^2}, \quad (17)$$

$$\alpha_{R1KP} = \alpha_{R1} \cos^2 \theta_{R1} = \alpha_{R1} \frac{1}{1 + \gamma_{R1}^2}, \quad (18)$$

$$\alpha_{A1KP} = \alpha_{A1} \frac{1}{1 + \gamma_1^2}, \quad (19)$$

$$\kappa = \frac{\gamma_1}{\sqrt{2\alpha_1} \cos(\theta_1)} = \frac{\gamma_1}{\gamma_C}, \quad (20)$$

$$\gamma_C = \tan(\theta_C), \quad (21)$$

where γ_C is the non-dimensional critical angle, and θ_C is the critical angle.

Therefore, we obtain (3142)-type ($0 < \kappa < 1$) as follows:

$$\alpha_{R1} = \kappa^2 \alpha_1 \frac{1 + \gamma_C^2}{1 + \kappa^2 \gamma_C^2}, \quad (22)$$

$$\gamma_{R1} = \gamma_C, \quad (23)$$

$$\alpha_{A1} = \alpha_1 (1 + \kappa^2)^2, \quad (24)$$

$$\gamma_w = \gamma_C \frac{1 - \kappa}{3}. \quad (25)$$

Also, we obtain O-type ($\kappa > 1$) as follows:

$$\alpha_{R1} = \alpha_1, \quad (26)$$

$$\alpha_{A1} = \alpha_1 \frac{4}{1 + \sqrt{1 - \kappa^{-2}}}. \quad (27)$$

B. Theoretical solutions for α_{A2} , α_{A3} , ... when $\gamma_1 < \gamma_C$ ($0 < \kappa < 1$)

When (3142)-type occurs due to the reflection from the oblique boundary ($0 < \kappa < 1$), the origin of the first solitary wave reflection detaches from the oblique boundary (Fig. 2). In such cases, the angle measured from the wall may be inadequate for deriving the theoretical solution for the soliton resonance. Thus, we rotate the propagation direction of the second and following resonances with an angle of θ_w . Therefore, the incident angles of the second solitary wave and the reflection of the first solitary wave are given as γ_2 and γ_{R2} (Fig. 2):

$$\gamma_2 = \tan(\theta_2) = \tan(\theta_1 + \theta_w), \quad (28)$$

$$\gamma_{R2} = \tan(\theta_{R2}) = \tan(\theta_C - \theta_w). \quad (29)$$

Since γ_2 is not equal to γ_{R2} , there may be two possibilities in regard to the modification angle for the modified Miles' prediction for γ_2 and γ_{R2} : $\cos(\theta_2)$ and $\cos(\theta_{R2})$ and the central angle $\cos[(\theta_2 + \theta_{R2})/2]$. We applied $\cos(\theta_2)$ and $\cos(\theta_{R2})$ to the modified Miles' prediction in this study. The applicability of two representative modification angles is investigated below in the Discussion section. If the soliton resonance between the second incident solitary wave and the reflection of the first solitary wave (the second soliton resonance in Fig. 2) is O-type, this satisfies $k_{1A} < k_{2A} < k_{3A} < k_{4A}$,

$$k_{1A} = -\frac{\gamma_2}{2} - \sqrt{\frac{\alpha_{2KP}}{2}}, \quad (30)$$

$$k_{2A} = -\frac{\gamma_2}{2} + \sqrt{\frac{\alpha_{2KP}}{2}}, \quad (31)$$

$$k_{3A} = \frac{\gamma_{R2}}{2} - \sqrt{\frac{\alpha'_{R1KP}}{2}}, \quad (32)$$

$$k_{4A} = \frac{\gamma_{R2}}{2} + \sqrt{\frac{\alpha'_{R1KP}}{2}}, \quad (33)$$

$$\alpha_{2KP} = \alpha_2 \cos^2 \theta_2 = \alpha_2 \frac{1}{1 + \gamma_2^2}, \quad (34)$$

$$\alpha'_{R1KP} = \alpha_{R1} \cos^2 \theta_{R2} = \alpha_{R1} \frac{1}{1 + \gamma_{R2}^2}. \quad (35)$$

To satisfy $k_{1A} < k_{2A} < k_{3A} < k_{4A}$, we require $k_{2A} < k_{3A}$. Assuming $\alpha_1 = 0.15$, we found that O-type appears in the range of $0.25 < \kappa < 1.0$ (Fig. 3). For $0 < \kappa < 0.25$, the non-dimensional amplitude of the first incident solitary wave α_1 should be much larger than the non-dimensional incident angle of the first solitary wave γ_1 . This raises the question of whether the "weakly nonlinear" KP theory can be applied to analyze soliton resonance. Therefore, we conjecture that KP theory will not significantly affect the soliton resonance in the range of $0 < \kappa < 0.25$. In the Discussion section, we investigate in detail whether some type of soliton resonance other than O-type appears in the range of $0 < \kappa < 0.25$.

The non-dimensional amplitude of the second soliton resonance α_{A2} is obtained as (36) in $0.25 < \kappa < 1.0$ (Kodama, 2010),

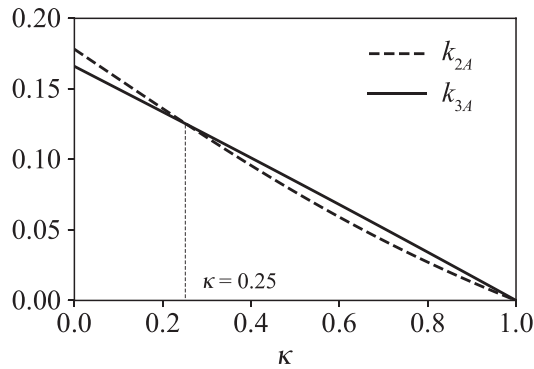


FIG. 3. Possibility of the occurrence of O-type and (3142)-type. k_{2A} and k_{3A} are shown for soliton resonance between the second incident solitary wave and the reflection of the first solitary wave when $\gamma_1 < \gamma_C$.

$$\alpha_{A2} = \frac{1}{1 + \sqrt{Y_A}} \left[\left(\sqrt{\alpha_{2KP}} + \sqrt{\alpha'_{R1KP}} \right)^2 + \sqrt{Y_A} \left(\sqrt{\alpha_{2KP}} - \sqrt{\alpha'_{R1KP}} \right)^2 \right], \quad (36)$$

$$Y_A = 1 - \frac{(k_{2A} - k_{1A})(k_{4A} - k_{3A})}{(k_{4A} - k_{2A})(k_{3A} - k_{1A})}. \quad (37)$$

Since the second soliton resonance is O-type in $0.25 < \kappa < 1.0$, the reflected wave reaches the third solitary wave without any deformation ($\alpha_{R2} = \alpha_{R1}$). When the non-dimensional amplitude of the third solitary wave α_3 is equal to α_2 , the same consideration can be applied to the third soliton resonance in Fig. 2. Therefore, we obtain the non-dimensional amplitude of the third soliton resonance α_{A3} by using (36). The other non-dimensional amplitudes of soliton resonances α_{A4}, \dots are thus given by using (36) by iteration.

C. Theoretical solutions for $\alpha_{A2}, \alpha_{A3}, \dots$ when $\gamma_1 > \gamma_C$ ($\kappa > 1$)

When O-type occurs due to the reflection from the oblique boundary ($\kappa > 1$), the incident angles of the second solitary wave and the reflection of the first solitary wave are γ_1 and γ_1 (Fig. 2). Therefore, the modification angle for the modified Miles' prediction is found to be $\cos(\theta_1)$ only.

$$\gamma_2 = \tan(\theta_2) = \gamma_1, \quad (38)$$

$$\gamma_{R2} = \tan(\theta_{R2}) = \gamma_1. \quad (39)$$

If the second soliton resonance is O-type, which satisfies $k_{1B} < k_{2B} < k_{3B} < k_{4B}$, then the coefficients are as follows:

$$k_{1B} = -\frac{\gamma_1}{2} - \sqrt{\frac{\alpha_{2KP}}{2}}, \quad (40)$$

$$k_{2B} = -\frac{\gamma_1}{2} + \sqrt{\frac{\alpha_{2KP}}{2}}, \quad (41)$$

$$k_{3B} = \frac{\gamma_1}{2} - \sqrt{\frac{\alpha_{1KP}}{2}}, \quad (42)$$

$$k_{4B} = \frac{\gamma_1}{2} + \sqrt{\frac{\alpha_{1KP}}{2}}. \quad (43)$$

To satisfy $k_{1B} < k_{2B} < k_{3B} < k_{4B}$, we stipulate $k_{2B} < k_{3B}$, which yields the condition of (44). The non-dimensional amplitude of the second solitary wave is smaller than that of the first solitary wave in a train of solitary waves (Horn *et al.*, 2000), which means $(\sqrt{\alpha_1} + \sqrt{\alpha_2})/2\sqrt{\alpha_1} < 1$. Because $\kappa > 1$, this satisfied (44), and the second soliton resonance is O-type theoretically. The non-dimensional amplitude of the second soliton resonance α_{A2} is obtained as (45) (Kodama, 2010). Since the second soliton resonances are O-type, α_{R2} is equal to α_{R1} . Therefore, we obtain the other non-dimensional amplitudes of soliton resonances $\alpha_{A3}, \alpha_{A4}, \dots$ by using (45):

$$\kappa > \frac{\sqrt{\alpha_1} + \sqrt{\alpha_2}}{2\sqrt{\alpha_1}}, \quad (44)$$

$$\alpha_{A2} = \frac{1}{1 + \sqrt{Y_B}} \left[\left(\sqrt{\alpha_{2KP}} + \sqrt{\alpha_{1KP}} \right)^2 + \sqrt{Y_B} \left(\sqrt{\alpha_{2KP}} - \sqrt{\alpha_{1KP}} \right)^2 \right], \quad (45)$$

$$Y_B = 1 - \frac{(k_{2B} - k_{1B})(k_{4B} - k_{3B})}{(k_{4B} - k_{2B})(k_{3B} - k_{1B})}. \quad (46)$$

III. NUMERICAL SIMULATION

A. Fully nonlinear and strongly dispersive model

We applied the FDI-2s to analyze multiple solitary wave interactions (Nakayama and Kakinuma, 2010; Nakayama *et al.*, 2019). The FDI-2s is based on the variational principle by following Luke (1967), and the velocity potential is expanded in a series of z , which showed that the vertical profile of horizontal velocity under a strong-nonlinear solitary wave could be evaluated accurately (Nakayama *et al.*, 2019). The flow is assumed to be incompressible, and it is considered that waves propagate in a stable two-layer inviscid fluid. The theoretical solution of the dispersion relationship for surface waves was compared with the linearized modified FDI-2s equation, which demonstrated the high applicability of the FDI-2s equation (Nakayama *et al.*, 2019). As other examples for applying the model based on the variational principle, Sakaguchi *et al.* (2020) demonstrated the high applicability of the fully nonlinear and strongly dispersive surface wave model (FDS) to surface waves by comparing its results to those from laboratory experiments. Nakayama and Lamb (2020) also applied the fully nonlinear and strongly dispersive internal wave model in a three-layer system (FDI-3s) to analyze breathers successfully. We attempted to use the FDI-2s to analyze multiple solitary wave interactions by considering that the upper and lower layers are air and water layers, respectively (Fig. 4). The equations of the FDI-2s are as follows:

[First layer]

$$\eta^\alpha \frac{\partial \eta}{\partial t} + \frac{1}{\alpha + \beta + 1} \nabla \left(\eta^{\alpha+\beta+1} \nabla f_{1,\beta} \right) - \frac{\alpha\beta}{\alpha + \beta - 1} \eta^{\alpha+\beta-1} f_{1,\beta} = 0, \quad (47)$$

$$\eta^\beta \frac{\partial f_{1,\beta}}{\partial t} + \frac{1}{2} \eta^{\beta+\gamma} \nabla f_{1,\beta} \nabla f_{1,\gamma} + \frac{\beta\gamma}{2} \eta^{\alpha+\beta-2} f_{1,\beta} \nabla f_{1,\gamma} + g\eta + \frac{p_1}{\rho_1} = 0, \quad (48)$$

$$\phi_1(x, y, z, t) = \sum_{\alpha=0}^{N-1} z^\alpha f_{1,\alpha}. \quad (49)$$

[Second layer]

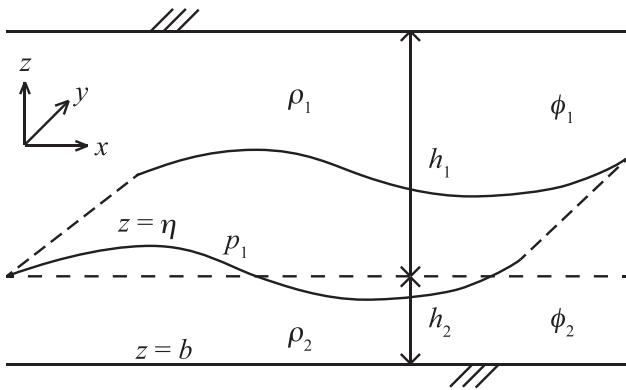


FIG. 4. Two-layer fluid in the FDI-2s. The upper and lower layers are air and water, respectively.

$$\eta^\alpha \frac{\partial \eta}{\partial t} + \frac{1}{\alpha + \beta + 1} \nabla \left[(\eta^{\alpha+\beta+1} - b^{\alpha+\beta+1}) \nabla f_{2,\beta} \right] - \frac{\alpha \beta}{\alpha + \beta - 1} (\eta^{\alpha+\beta-1} - b^{\alpha+\beta-1}) f_{2,\beta} = 0, \quad (50)$$

$$\eta^\beta \frac{\partial f_{2,\beta}}{\partial t} + \frac{1}{2} \eta^{\beta+\gamma} \nabla f_{2,\beta} \nabla f_{2,\gamma} + \frac{\beta \gamma}{2} \eta^{\alpha+\beta-2} f_{2,\beta} \nabla f_{2,\gamma} + g \eta + \frac{p_1 + (\rho_2 - \rho_1) g h_1}{\rho_2} = 0, \quad (51)$$

$$\phi_2(x, y, z, t) = \sum_{\alpha=0}^{N-1} z^\alpha f_{2,\alpha}, \quad (52)$$

where η is the water surface level, g is the gravitational acceleration, $\nabla = (\partial/\partial x, \partial/\partial y)$, ϕ_1 , and ϕ_2 are the velocity potential for the upper and lower layers, $f_{1,\alpha}$ and $f_{2,\alpha}$ are the coefficients of the power function for ϕ_1 and ϕ_2 , p_1 is the pressure at the water surface, N is the total number of an expanded function, h_1 and h_2 are the undisturbed water depth in the upper and lower layers, $\alpha = 1, 2, \dots, N$, $\beta = 1, 2, \dots, N$, and $\gamma = 1, 2, \dots, N$. ρ_1 and ρ_2 are the density of air and water, respectively, and the bottom is at $z = b$.

For the analysis of multiple solitary waves, three sequential solitary waves were applied in the numerical simulation. The spatial interval between solitary waves was given as 50.0 m to prevent the interaction among solitary waves. The depths of the upper and lower layers were given as 4.0 and 2.0 m. The same amplitude ($=0.2$ m) was applied to all solitary waves, and we used nine different incident angles in the simulation (Table I). The mesh grid interval, $\Delta x = 1.0$ m, $\Delta y = 1.0$ m, and the time step, $\Delta t = 0.0005$ s, were used in the numerical simulations. The Courant–Friedrichs–Lewy condition was 0.00221 based on the linear theory, which was small enough to apply the variational principle (Nakayama *et al.*, 2019). To reduce the runtime cost, we carried out computations by using a moving computational domain, in which the maximum active computational area is 400×500 m for the x and y coordinates. A sponge layer was applied on the left boundary of the moving computational area to remove the reflection from the left edge. Parallel computation was conducted using 12 central processing units with openMP until the simulation reached a steady-state condition. The oblique boundary condition was satisfied by applying the normal velocity zero condition of Simanjuntak *et al.* (2009).

TABLE I. Main parameters for numerical simulations.

Case	θ_1	θ_C	κ	α_{A1}/α_1	α_{A2}/α_1	α_{A3}/α_1
1	15	27.7	0.51	2.34	1.82	1.65
2	20	27.1	0.71	2.90	2.35	2.15
3	23	26.6	0.85	3.32	2.72	2.51
4	25	26.3	0.94	3.62	3.05	2.85
5	26	26.1	0.99	3.70	3.22	3.02
6	27	25.9	1.05	3.34	3.16	2.97
7	29	25.5	1.16	2.72	2.73	2.70
8	33	24.6	1.42	2.37	2.36	2.31
9	40	22.7	2.00	2.15	2.15	2.10

B. Comparisons with theoretical solutions

The critical amplitudes γ_C for all cases were obtained from (21), which classified that cases 1–5 were (3142)-type and cases 6–9 were O-type, respectively (Table I). In numerical simulations, Mach stem was confirmed to occur at the first soliton resonance from the oblique boundary in cases 1–5, which corresponded to (3142)-type [Figs. 5(a)–5(c) and 6(a)–6(c)]. When $k < 1$, the smaller the incident angle, the less the time to reach a steady-state [Figs. 5(a)–5(c)]. In contrast, there was no Mach stem at the first soliton resonance, and the amplified amplitude at the oblique boundary decreased with the increase in θ_1 in cases 6–9, which corresponded to O-type [Figs. 5(d)–5(f) and 6(d)–6(f)]. When $k > 1$, the larger the incident angle, the less the time to reach a steady-state [Figs. 5(d)–5(f)]. Additionally, it was confirmed that the duration to reach a steady-state is relatively longer in Mach stem cases than no Mach stem cases (Fig. 5). Case 5 required the most time to reach the steady-state because the θ_1 of case 5 was the closest to the critical angle, which was also revealed by Nakayama *et al.* (2019).

In cases 1–5, where (3142)-type occurs ($0 < \kappa < 1$), the non-dimensional amplitude of the computed first soliton resonance α_{A1} agreed with the theoretical solutions (24), while the numerical simulations were slightly smaller around $\kappa \approx 1$ [Fig. 7(a)]. In cases 6–9, where O-type occurs ($\kappa > 1$), α_{A1} agreed with the theoretical solutions (27) very well [Fig. 7(a)]. Regarding the non-dimensional amplitude of the reflection of the first solitary wave α_{R1} , the numerical simulations agreed with the theoretical solutions (22) and (26), while the numerical simulations were larger slightly when $\kappa > 1$ (Fig. 8).

In regard to the non-dimensional amplitude of the second soliton resonance α_{A2} , we found no stem-like wave in cases 1–5, which means that the soliton resonance was O-type (Fig. 6). We expected O-type at the second soliton resonance for $0.25 < \kappa < 1$ from Fig. 3, which was thus validated by using numerical simulations. In cases 6 to 9, where $\kappa > 1$, the second soliton resonance was confirmed to be O-type (Fig. 6). We obtained good agreements of α_{A2} between the numerical simulations and theoretical solutions (36) and (45), although the computed α_{A2} was slightly smaller than the theoretical one around $\kappa \approx 1$ [Fig. 7(b)]. Regarding α_{A3} , there was no stem-like wave at the third soliton resonance in all cases 1–9 (Fig. 6). Third soliton resonance was thus confirmed to be O-type in all cases as we expected from the theory. α_{A3} was slightly smaller than α_{A2} , and agreed well with the theoretical solutions (36) and (45), though the computed α_{A3} was also slightly smaller than the theoretical one.

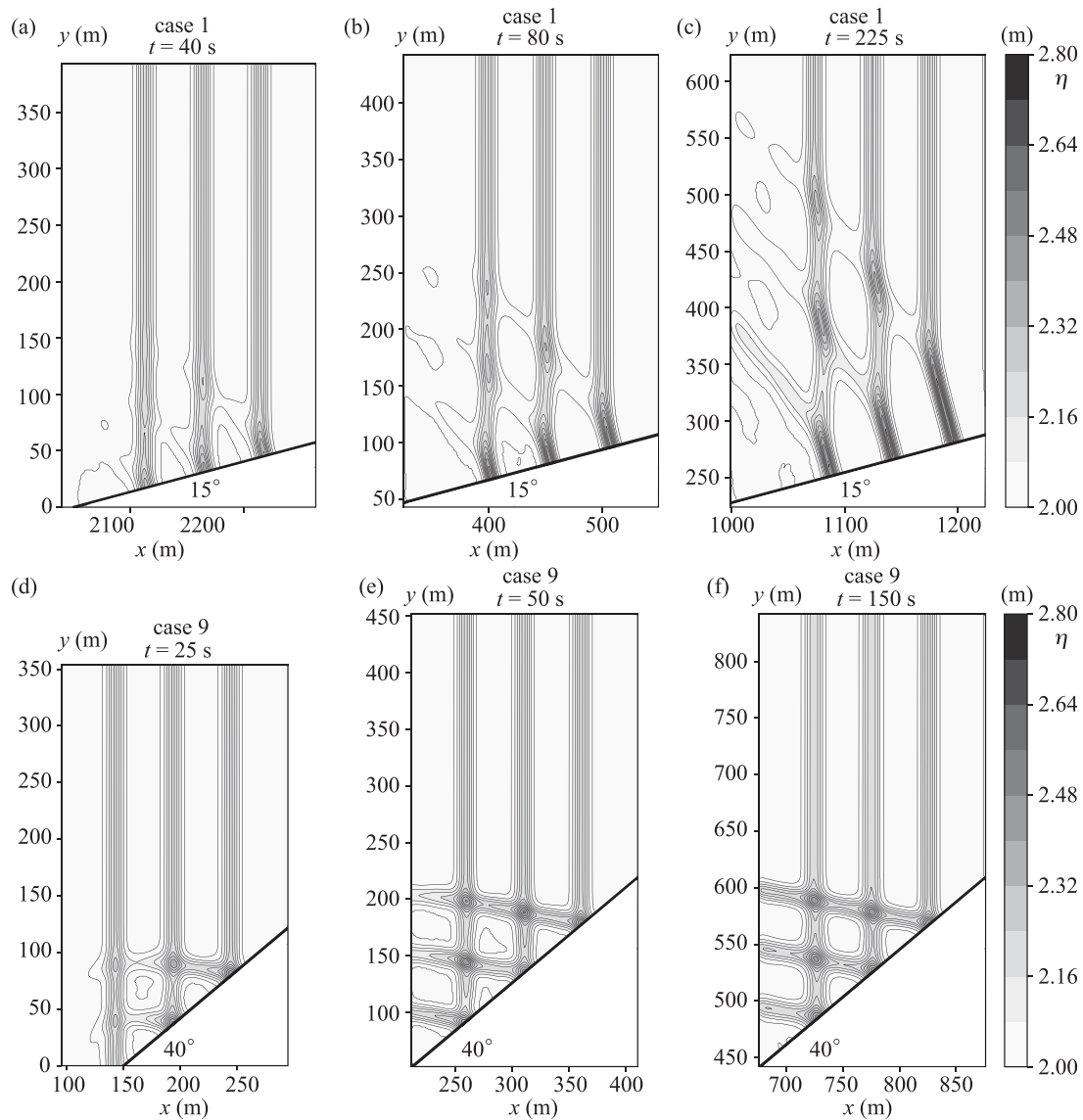


FIG. 5. Horizontal distribution of water depth by numerical simulations. Case 1: $\theta_1 = 15^\circ$ at (a) $t = 40$ s, (b) $t = 80$ s, and (c) $t = 225$ s. Case 9: $\theta_1 = 40^\circ$ at (d) $t = 25$ s, (e) $t = 50$ s, and (f) $t = 150$ s.

The non-dimensional amplitude α_{R2} agreed well with the theoretical solution (22) in $0 < \kappa < 1$ (Fig. 8). In $\kappa > 1$, α_{R2} was confirmed to be similar to α_1 , which agreed with the theoretical solution (26) (Fig. 8). In addition, with respect to the non-dimensional amplitude α_{R3} , the numerical simulations agreed well with the theoretical solutions (22) and (26). Interestingly, α_{R2} was found to be slightly smaller than α_{R1} . Additionally, α_{R3} was smaller than α_{R2} . As shown above in the comparisons between α_{A2} and α_{A3} , α_{A3} was smaller than α_{A2} . Since the FDI-2s can include the effect of full nonlinearity on the computation of soliton resonance, we conjecture that consecutive soliton resonances reduce the potential or kinetic energy, which results in the decreases in α_{A3} , α_{R2} , and α_{R3} .

IV. DISCUSSION

Funakoshi (1980) showed that the Boussinesq equation model well-reproduced soliton resonance due to the interaction of an incident solitary wave with the oblique boundary by giving a small amplitude solitary wave. The computed amplification factors were slightly smaller than the Miles' prediction around $\kappa \approx 1$, suggesting that the computational results may not have reached the steady-state. On the otherhand, Tanaka (1993) found that the maximum amplification factor was about three times as large as the solitary incident wave based on the finding that it gave a large-amplitude solitary wave. Yeh *et al.* (2010) also demonstrated that the maximum fourfold amplification predicted by Miles was not realized under strong nonlinear condition.

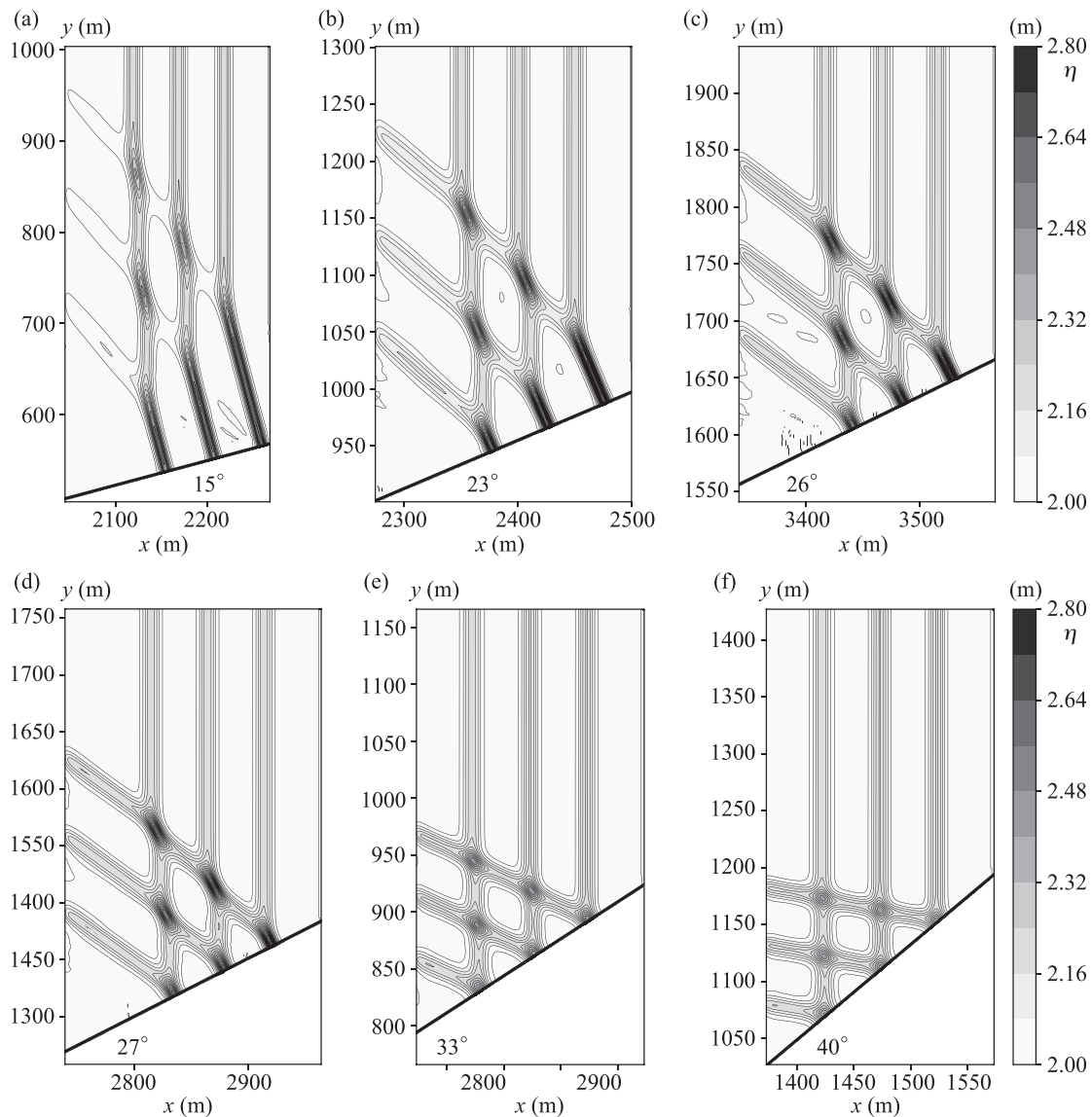


FIG. 6. Horizontal distribution of water depth by numerical simulations. (a) Case 1: $\theta_1 = 15^\circ$ at $t = 450$ s. (b) Case 3: $\theta_1 = 23^\circ$ at $t = 500$ s. (c) Case 5: $\theta_1 = 26^\circ$ at $t = 730$ s. (d) Case 6: $\theta_1 = 27^\circ$ at $t = 600$ s. (e) Case 8: $\theta_1 = 33^\circ$ at $t = 300$ s. (f) Case 9: $\theta_1 = 40^\circ$ at $t = 300$ s.

Nakayama *et al.* (2019) showed a similar suppression of amplification factors when the amplitude of a solitary incident wave was relatively large, while their target was the interaction of internal solitary waves. Since the maximum amplitude of a solitary wave is about 80% of the total water depth ($a_{A1} = 0.8h_2$) (McCowan, 1894), the possible non-dimensional amplitude of the first soliton resonance α_{A1} is expected to be about 1.2 $[= 3a_{A1}/(2h_2)]$. As the maximum amplification factor is 4, we can give the non-dimensional amplitude of the first solitary wave α_1 up to about 0.3 $[= 3a_1/(2h_2)]$ in numerical simulations. In the present study, we applied $\alpha_1 = 0.15$, which is half as large as the potential maximum. Therefore, nonlinearity was less, and we obtained similar results as Funakoshi (1980) [Fig. 7(a)].

We obtained good agreements in regard to the normalized amplitudes of the second and third resonances (α_{A2}/α_1 and α_{A3}/α_1) between numerical simulations and theoretical solutions by applying $\cos(\theta_2)$ and $\cos(\theta_{R2})$ to the modified Miles' prediction in $0 < \kappa < 1$ [Fig. 7(b)]. However, there is another possible means of improving Miles' prediction, i.e., by using $\cos[(\theta_2 + \theta_{R2})/2]$, presuming that the second resonance propagates with an incident angle of $(\theta_2 + \theta_{R2})/2$. Therefore, we investigated the change in the theoretical solution (36) by using two different modification angles, which showed that there is no significant difference between $\cos(\theta_2)$ and $\cos(\theta_{R2})$ and $\cos[(\theta_2 + \theta_{R2})/2]$ (Fig. 9). However, both theoretical solutions overestimated the numerical computations around $\kappa \approx 1$. In the case of

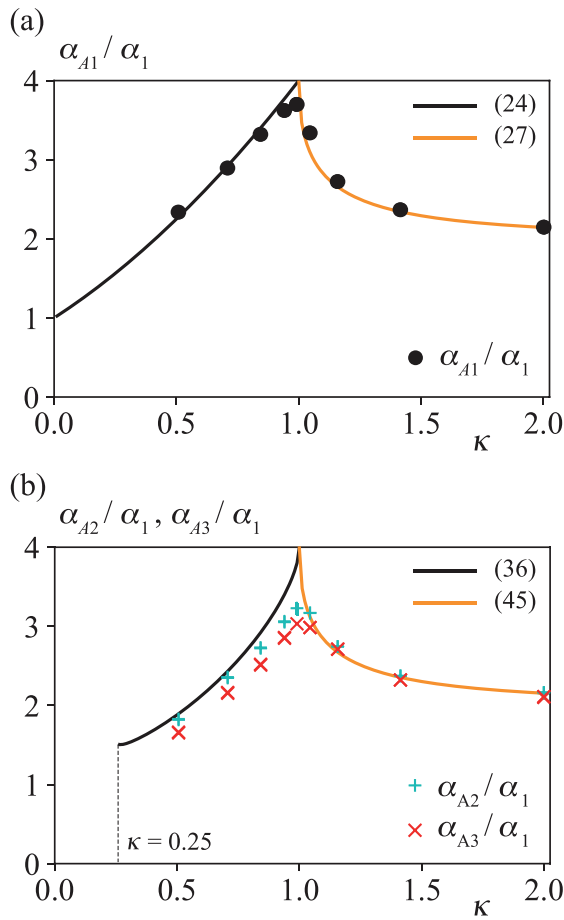


FIG. 7. Normalized amplitude of the theoretical solution and numerical simulation. (a) κ and α_{A1}/α_1 . (b) κ and α_{A2}/α_1 and α_{A3}/α_1 .

$\cos[(\theta_2 + \theta_{R2})/2]$, O-type was revealed to occur in $0.21 < \kappa < 1.0$, which means that the other type of soliton resonance may appear in $0 < \kappa < 0.21$. In addition, we investigated the effect of the non-dimensional amplitude of the first solitary wave α_1 on the theoretical solution (36). We found that the smaller the α_1 , the closer to (24) the theoretical solution (36) moves. Still, the range of O-type is $0.25 < \kappa < 1.0$. Note that α_{2A}/α_1 is 4 in $0 < \kappa < 1.0$ if we ignore modification angles and the angle due to extension of the Mach stem when $\alpha_2 = \alpha_1$, which is not realistic and shows the necessity of considering the modification angles and the effect of extension of the Mach stem.

As shown in Figs. 7 and 9, there is a possibility that the second soliton resonance is of the other type when κ is relatively small. Kodama (2010) revealed the potential of the occurrence of O-type, (3142)-type, and (4321)-type (P-type) when two solitons interact. The present study investigated whether (3142)-type and P-type occur when we apply $\cos(\theta_2)$ and $\cos(\theta_{R2})$ to the modified Miles' prediction in $0 < \kappa < 0.25$. First, if the second soliton resonance is (3142)-type, $k_{2A(3142)} < k_{3A(3142)}$ should be satisfied,

$$k_{2A(3142)} = \frac{\gamma_{R2}}{2} - \sqrt{\frac{\alpha_{R1KP}}{2}}, \quad (53)$$

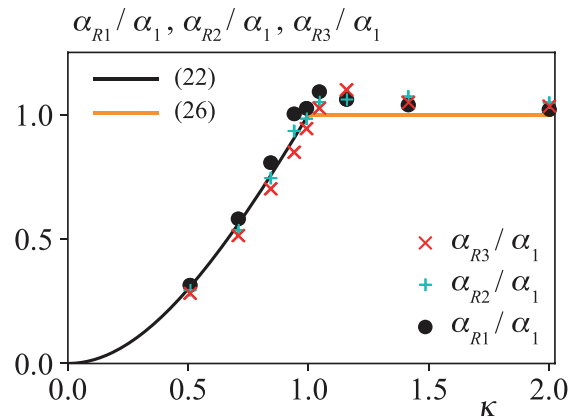


FIG. 8. Normalized amplitude of the theoretical solution and numerical simulation. κ and α_{R1}/α_1 , α_{R2}/α_1 , and α_{R3}/α_1 .

$$k_{3A(3142)} = -\frac{\gamma_2}{2} + \sqrt{\frac{\alpha_{2KP}}{2}}. \quad (54)$$

Second, if the second soliton resonance is P-type, $k_{1A(4321)} < k_{2A(4321)}$ and $k_{3A(4321)} < k_{4A(4321)}$ should be satisfied,

$$k_{1A(4321)} = -\frac{\gamma_2}{2} - \sqrt{\frac{\alpha_{2KP}}{2}}, \quad (55)$$

$$k_{2A(4321)} = k_{2A(3142)} = \frac{\gamma_{R2}}{2} - \sqrt{\frac{\alpha_{R1KP}}{2}}, \quad (56)$$

$$k_{3A(4321)} = \frac{\gamma_{R2}}{2} + \sqrt{\frac{\alpha_{R1KP}}{2}}, \quad (57)$$

$$k_{4A(4321)} = k_{3A(3142)} = -\frac{\gamma_2}{2} + \sqrt{\frac{\alpha_{2KP}}{2}}. \quad (58)$$

It is evident that $k_{1A(4321)} < k_{2A(4321)} < k_{3A(4321)}$ is satisfied in $0 < \kappa < 0.25$. Therefore, we investigated $k_{2A(3142)} < k_{3A(3142)}$ for (3142)-type and $k_{3A(4321)} < k_{4A(4321)}$ for P-type, respectively.

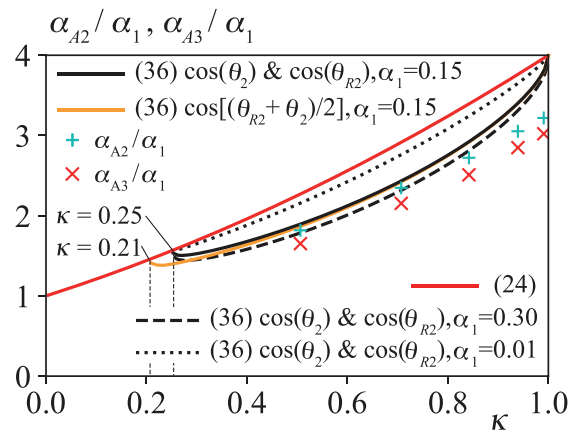


FIG. 9. Normalized amplitude of the theoretical solution and numerical simulation. κ and α_{A2}/α_1 and α_{A3}/α_1 .

Regarding (3142)-type, $k_{2A(3142)} < k_{3A(3142)}$ was found to be satisfied, which shows the possibility of the occurrence of (3142)-type in $0 < \kappa < 0.25$ (Fig. 10). In contrast, $k_{3A(4321)} < k_{4A(4321)}$ was revealed to be satisfied in $0 < \kappa < 0.021$, which shows the limitation of the occurrence range of P-type (Fig. 10). Thus, we conjecture that soliton resonance is (3142)-type in $0.021 < \kappa < 0.25$ and (3142)-type or P-type in $0 < \kappa < 0.021$. We cannot determine whether (3142)-type or P-type occurs in $0 < \kappa < 0.021$ uniquely. To let $\kappa \approx 0$, the amplitude of the first solitary wave α_1 must be very large or the non-dimensional incident angle of the first solitary wave γ_1 must be very small, which may not satisfy the “weakly nonlinear” KP theory. Additionally, the non-dimensional amplitude of the second soliton resonance α_{A2} is expected to be similar to the non-dimensional amplitude of the second solitary wave α_2 around $\kappa \approx 0$, which suggests that weakly nonlinear KP theory will not significantly affect the soliton resonance in the range of $0 < \kappa < 0.25$.

In a train of solitary waves, the amplitudes gradually decrease from the front toward the end. Therefore, we investigated how the non-dimensional amplitude of the second soliton resonance α_{A2} varies by changing the non-dimensional amplitude of the second solitary wave α_2 . We set $\alpha_2 = 2\alpha_1/3$ and $\alpha_2 = \alpha_1/3$. When $\alpha_2 = 2\alpha_1/3$, $k_{2A} < k_{3A}$ was revealed to be satisfied in $\kappa > 0$, which suggests that the second soliton resonance is O-type [Fig. 11(a)]. Significantly, O-type at the second soliton resonance was confirmed to be valid for the values of α_1 from 0.15 to 0.30 when $\alpha_2 \ll \alpha_1$. Thus, the second and the subsequent soliton resonances were found to be O-type when $\alpha_2 \ll \alpha_1$, and their non-dimensional amplitudes could be obtained by using the theoretical solutions (36) and (45). In the previous study related to internal waves, Zheng *et al.* (1995) showed that the second and the subsequent soliton resonances due to a train of internal solitary waves were O-type. Moreover, we found that the amplification factor of the second soliton resonance α_{A2} decreases with the decrease in α_2 [Fig. 11(b)]. In the present study, we applied a non-dimensional amplitude of the first solitary wave α_1 to calculate an amplification factor, and we did not use a normalized non-dimensional amplitude (59). By using (59), the maximum amplification factor becomes fourfold when $\alpha_2 \ll \alpha_1$ and $\kappa = 1$:

$$\alpha_{m2KP} = \frac{(\sqrt{\alpha_{2KP}} + \sqrt{\alpha_{R1KP}})^2}{4}, \quad (59)$$

where α_{m2} is the normalized amplitude of α_2 and α_{R1} .

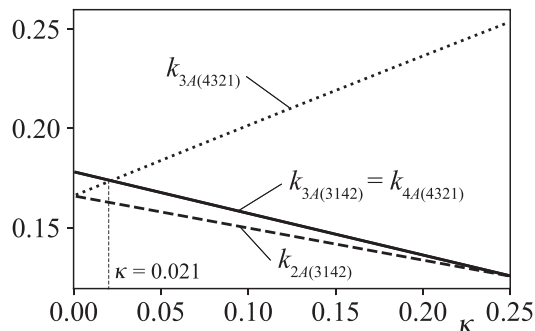


FIG. 10. Possibility of the occurrence of (3142)-type and P-type. κ and $k_{2A(3142)}$, $k_{3A(3142)}$, $k_{3A(4321)}$, and $k_{4A(4321)}$ when $0 < \kappa < 0.06$.

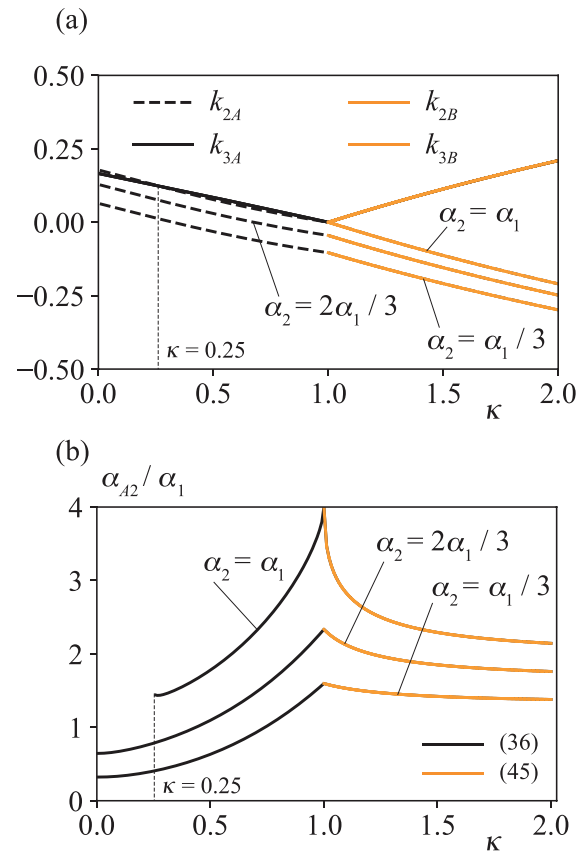


FIG. 11. Amplification factors when the second incident amplitude varies. $\alpha_2 = \alpha_1/3$, $2\alpha_1/3$ and α_1 . (a) κ and k_{2A} , k_{3A} , k_{2B} , and k_{3B} . (b) κ and α_{A2}/α_1 .

V. CONCLUSIONS

The first soliton resonance from the oblique boundary was well-reproduced by using the FDI-2s. The amplification factors of the first soliton resonance agreed well between the theoretical solutions and numerical simulations. Also, the computed amplification factors of the second and the third soliton resonances agreed with the theoretical solutions. In $0.25 < \kappa < 1$, the second and the subsequent soliton resonances were found to be O-type. The modification angle for the modified Miles' prediction was suggested to be $\cos(\theta_2)$ and $\cos(\theta_{R2})$ for the second resonance. In $\kappa > 1$, all soliton resonances were O-type. The second soliton resonance was (3142)-type in $0.021 < \kappa < 0.25$ and (3142)-type or P-type in $0 < \kappa < 0.021$. The amplitude of the second soliton resonance is expected to be similar to the second solitary wave around $\kappa \approx 0$, which suggests that KP theory will not significantly affect the soliton resonance in the range of $0 < \kappa < 0.25$. Therefore, disregarding the type of the first soliton resonance, the second and the subsequent soliton resonances were revealed to be O-type, which indicates that the amplification factor can be estimated by using the theoretical solutions proposed in this study. However, the aim of the present study was limited to clarifying the interactions of multiple solitary waves by using the oblique boundary; further research will be needed to investigate the interactions of multiple solitary waves with different amplitudes.

AUTHORS' CONTRIBUTIONS

K.N. designed all the numerical computations, wrote most of the paper, and performed all the analyses. H.T. discussed the investigation with K.N.

ACKNOWLEDGMENTS

This work was supported by the Japan Society for the Promotion of Science under Grant Nos. 18H01545 and 18KK0119. This work was also supported in part by the Collaborative Research Program of the Research Institute for Applied Mechanics, Kyushu University.

DATA AVAILABILITY

The data that support the findings of this study are available from the corresponding author upon reasonable request.

REFERENCES

- Aghsaee, P., Boegman, L., and Lamb, K. G., "Breaking of shoaling internal solitary waves," *J. Fluid Mech.* **659**, 289–317 (2010).
- Arthur, R. S., and Fringer, O. B., "The dynamics of breaking internal solitary waves on slopes," *J. Fluid Mech.* **761**, 360–398 (2014).
- Funakoshi, M., "Reflection of obliquely incident solitary waves," *J. Phys. Soc. Jpn.* **49**, 2371–2379 (1980).
- Gidel, F., Bokhove, O., and Kalogirou, A., "Variational modelling of extreme waves through oblique interaction of solitary waves: application to Mach reflection," *Nonlin. Processes Geophys.* **24**, 43–60 (2017).
- Helfrich, K. R., and Melville, W. K., "Long nonlinear internal waves," *Annu. Rev. Fluid Mech.* **38**, 395–425 (2006).
- Horn, D. A., Imberger, J., Ivey, G. N., and Redekopp, L. G., "A weakly nonlinear model of long internal waves in closed basins," *J. Fluid Mech.* **467**, 269–287 (2002).
- Horn, D. A., Redekopp, L. G., Imberger, J., and Ivey, G. N., "Internal wave evolution in a space-time varying field," *J. Fluid Mech.* **424**, 279–301 (2000).
- Kharif, C., and Pelinovsky, E., "Physical mechanisms of the rogue wave phenomenon," *Eur. J. Mech. B/Fluids* **22**, 603–634 (2003).
- Kodama, Y., "KP solitons in shallow water," *J. Phys. A* **43**, 434004 (2010).
- Kodama, Y., "The KP theory and Mach reflection," *J. Fluid Mech.* **800**, 766–786 (2016).
- Li, W., Yeh, H., and Kodama, Y., "On the Mach reflection of a solitary wave: Evisited," *J. Fluid Mech.* **672**, 326–357 (2011).
- Luke, J. C., "A variational principle for a fluid with a free surface," *J. Fluid Mech.* **27**, 395–397 (1967).
- Maxworthy, T., "On the formation of nonlinear internal waves from the gravitational collapse of mixed regions in two and three dimensions," *J. Fluid Mech.* **96**, 47–64 (1980).
- McCowan, J., "On the highest wave of permanent type," *Philos. Mag.* **38**(5), 351–358 (1894).
- Melville, W. K., "On the Mach reflection of a solitary wave," *J. Fluid Mech.* **98**, 285–297 (1980).
- Miles, J. W., "Resonantly interacting solitary waves," *J. Fluid Mech.* **79**, 171–179 (1977).
- Nakayama, K., "Comparisons of using CIP, compact and CIP-CSL2 schemes for internal solitary waves," *Int. J. Numer. Methods Fluids* **51**, 197–219 (2006).
- Nakayama, K., and Lamb, K., "Breathers in a three-layer fluid," *J. Fluid Mech.* **903**, 40 (2020).
- Nakayama, K., and Kakinuma, T., "Internal waves in a two-layer system using fully nonlinear internal-wave equations," *Int. J. Numer. Methods Fluids* **62**, 574–590 (2010).
- Nakayama, K., Shimizu, K., Kakinuma, T., and Tsuji, E., "Analysis of resonance of solitary wave trains using fully nonlinear and strongly dispersive wave equations," *J. Jpn. Soc. Civil Eng., Ser. B2* **72**(2), 7–12 (2016).
- Nakayama, K., Kakinuma, T., and Tsuji, H., "Oblique reflection of large internal solitary wave," *Eur. J. Mech. B/Fluids* **74**, 81–91 (2019).
- Nakayama, K., Sato, T., Shimizu, K., and Boegman, L., "Classification of internal solitary wave breaking over a slope," *Phys. Rev. Fluids* **4**, 014801 (2019).
- Peterson, P., Soomere, T., Engelbrecht, J., and van Groesen, E., "Soliton interaction as a possible model for extreme waves," *Nonlinear Processes Geophys.* **10**, 503–510 (2003).
- Sakaguchi, S., Nakayama, K., Vu, T. T. T., Komai, K., and Nielsen, P., "Nonlinear wave equations for free surface flow over a bump," *Coastal Eng. J.* **62**, 159–169 (2020).
- Shimizu, K., and Nakayama, K., "Effects of topography and earth's rotation on the oblique interaction of internal solitary-like waves in the Andaman Sea," *J. Geophys. Res.* **122**, 7449–7465, <https://doi.org/10.1002/2017JC012888> (2017).
- Simanjuntak, M. A., Imberger, J., and Nakayama, K., "Numerical wave drag due to stair-step topography in a geophysical flow model," *J. Geophys. Res.* **114**, C12020, <https://doi.org/10.1029/2008JC005051> (2009).
- Soomere, T., and Engelbrecht, J., "Extreme elevations and slopes of interacting solitons in shallow water," *Wave Motion* **41**(2), 179–192 (2005).
- Tanaka, M., "Mach reflection of a large-amplitude solitary wave," *J. Fluid Mech.* **248**, 637–661 (1993).
- Tsuji, H., and Oikawa, M., "Oblique interaction of solitons in an extended Kadomtsev-Petviashvili equation," *J. Phys. Soc. Jpn.* **76**, 084401–084408 (2007).
- Wang, C., and Pawlowicz, R., "Oblique wave-wave interactions of nonlinear near surface internal waves in the Strait of Georgia," *J. Geophys. Res.* **117**, C06031 (2012).
- Xue, J., Graber, H. C., Lund, B., and Romeister, R., "Satellite observation of a zipper-like internal waves-wave interaction pattern in the mid-Atlantic Bight," *IEEE International Symposium on Geoscience and Remote Sensing (IGARSS)* (IEEE, 2013), pp. 1571–1574.
- Yeh, H., Li, W., and Kodama, Y., "Mach reflection and KP solitons in shallow water," *Eur. Phys. J. Spec. Top.* **185**, 97–111 (2010).
- Zheng, Q., Klemas, V., and Yan, X. H., "Dynamic interpretation of space shuttle photographs: Deepwater internal waves in the western equatorial Indian Ocean," *J. Geophys. Res.* **100**, 2579–2589, <https://doi.org/10.1029/94JC02921> (1995).